Thin–Walled Structures 216 (2025) 113742

Contents lists available at ScienceDirect

Thin-Walled Structures

journal homepage: www.elsevier.com/locate/tws

Parametric study of a cold-formed steel profile employed in composite ribbed slabs

André V.S. Gomes [a,b,*], Daniel C.M. Candido [a], Lucas F. Favarato [a], Johann A. Ferrareto [c], Juliana C. Vianna [a], Adenilcia F.G. Calenzani [a]

[a] Federal University of Espírito Santo, Civil Engineering Graduate Program, Fernando Ferrari Avenue, 514, 29.060-970, Vitória, ES, Brazil
[b] ArcelorMittal Tubarão – Flat Carbon Steel, Brigadeiro Eduardo Gomes Avenue, 526, Pólo Industrial de Tubarão, 29.160-904, Serra, ES, Brazil
[c] ArcelorMittal Construction, France. 16 Route de La Forge, F – 55000, Hairon Ville, France

ARTICLE INFO

Keywords:
Numerical analysis
Cold-formed steel structures
Trelifácil® solution
Finite element modelling

ABSTRACT

Structural systems comprised by prefabricated flooring systems and/or cold-formed steel members are frequently employed in the construction industry due to their versatility, high strength-to-weight ratio, ease of prefabrication, transportation and assembly on site. The unification of these structural systems motivated the creation of composite ribbed slabs, which were defined in this research as ribbed floor systems in which cold-formed steel members are used as joists, and the space between them is filled with inert elements, so called Trelifácil® solution. The focus of this research is to develop parametric studies to examine the flexural capacity and stiffness of the cold-formed profile used in the Trelifácil® solution. A finite element model using ANSYS® 2020R1 was developed and validated with experimental tests to predict the flexural behaviour of the Trelifácil® solution and perform such analysis. Additionally, a finite element model for the entire configuration of the Trelifácil® solution is developed to study the interaction between the trussed reinforcement and the cold-formed steel member.

1. Introduction

In the last decades, the construction industry has greatly progressed by seeking more efficient and economical solutions. In this context, prefabricated structural systems play a significant role since they are manufactured in a controlled environment and present fast installation. Among them, steel lattice girders and cold-formed steel (CFS) structures are highlighted in this research. Lattice girders are usually used in prefabricated flooring systems of small and medium-sized constructions and have been, since their inception, an accessible option due to their simple construction techniques. Cold-formed steel members, in turn, may reduce the cost of structures as a result of their lower weight, relatively easy method of manufacturing, fast assembly, easy transportation and handling, high strength and stiffness, and others, when compared to materials such as timber and concrete.

Finite element (FE) models validated by measured data are commonly employed to assess the strength and stiffness of CFS profiles [1–3]. Torabian, Zheng and Schafer [1], for example, conducted a numerical and experimental study of seventeen 30.5 cm CFS profile specimens under combined influence of bi-axial bending moment and compression. The research also presents a parametric numerical analysis using the software ABAQUS. In closure, the numerical results are validated by the experiments and compared to limit state design (LSD) equations prescribed in the North American standard AISI-S100-12 [4]. This research is expanded in Torabian, Zheng and Schafer [2] by the inclusion of experimental and numerical tests of two additional member lengths, 61 cm and 122 cm. Both studies indicate that, in comparison with test results, standardized equations from the American code AISI-S100-12 are overly simplistic and conservative.

Moreover, such numerical models grounded on measured data are commonly used to conduct advanced studies that would be laborious and costly if performed in laboratories. Kumar and Sahoo [5], for example, calculated the moment capacity of multiple “U” and stiffened “U” CFS profile sections by means of standardized design equations and compared the results with a finite element analysis performed with ABAQUS. For validation, the numerical results are compared with the

* Corresponding author at: ArcelorMittal Tubarão – Flat Carbon Steel, Brigadeiro Eduardo Gomes Avenue, 526, Pólo Industrial de Tubarão, 29.160-904, Serra, ES, Brazil.

E-mail addresses: andrevsg91@hotmail.com, andre.vs.gomes@arcelormittal.com.br (A.V.S. Gomes), danielcandido89@gmail.com (D.C.M. Candido), lucasffavarato@gmail.com (L.F. Favarato), johann.ferrareto@arcelormittal.com (J.A. Ferrareto), jcvianna30@gmail.com (J.C. Vianna), afcalenzani@gmail.com (A.F.G. Calenzani).

https://doi.org/10.1016/j.tws.2025.113742
Received 28 February 2025; Received in revised form 20 May 2025; Accepted 18 July 2025
Available online 19 July 2025
0263-8231/© 2025 Elsevier Ltd. All rights are reserved, including those for text and data mining, AI training, and similar technologies.

behavior of selected profile sections, subjected to four-point flexure experiments about the minor axis of inertia. The last step of the research consisted of an applicability analysis of the standardized equations as function of width-to-thickness ratio, lip lengths and depth-to-width ratio of CFS profiles under minor axis bending, using the numerical results as a reference point.

In computational analysis FE models using shell elements have presented satisfactory results to simulate the nonlinear behavior of CFS profiles, while the Direct Strength Method (DSM) proposed by Schafer [6] is a consolidated alternative for estimating the ultimate strength of a member based on semi-empirical strength curves. Examples of studies where shell finite element models and/or the DSM were employed to numerically predict the strength behavior of CFS members can be found in [1,7–10].

Oey and Papangelis [11] investigated the behaviour of 33 cold-formed steel U-profiles under bending about the minor axis, inducing local buckling in the web. This was done through elastic buckling analyses using the strip method and nonlinear finite element analyses (NLFEA). The performance of the current DSM design equation was initially assessed against EWM and NLFEA results, revealing that the DSM equation is highly conservative for U-profiles bent about the minor axis. Based on the NLFEA results, an equation was derived linking the ultimate moment to the yield moment and elastic buckling moment for U-sections bent around the minor axis. A reliability analysis showed that the proposed design equation has good reliability.

Gkantou, Bock and Theofanous [12] conducted a detailed numerical analysis of the response of stainless steel I and C sections under bending about the minor axis, with flanges subjected to stress gradients. The developed numerical model was validated with experimental data from the literature on stainless steel sections. The results indicate that the current Class 3 limits in the Eurocode for AL elements are overly conservative, suggesting that these limits could be adjusted, as sections with flange slenderness up to 40 for I-sections and 30 for C-sections still maintain their elastic moment capacity. The DSM evaluation showed conservative predictions. To address this limitation, the effective plastic width method for hot-rolled and cold-formed steel, was adapted for stainless steel I-sections, and new equations were formulated to capture the effective plastic width in slender C-sections.

He, Dai and Ren [13] investigated the buckling of cold-formed, stiffened U-profiles under combined compression and bending about the minor axis. They developed finite element (FE) models, which were validated using available experimental tests. Following this, parametric analyses were performed to examine the influence of eccentricity on collapse modes and load-bearing capacity. It was found that the ultimate strength is influenced by different types of initial imperfections, with local imperfections reducing capacity more when eccentricity is directed towards the web, while distortional imperfections have a greater impact when directed towards the stiffened flange. Numerical results were compared to design strengths calculated using the EN 1993-1-3 [14], showing that the standard's interaction curve is conservative. Additionally, DSM curves were found to overestimate the predicted strength. To address this, modified DSM curves were proposed, incorporating the interaction effects between buckling modes, leading to more accurate load capacity predictions for stiffened U-profiles.

Kim *et al.* [15] experimentally investigated the bending performance of a new steel-concrete composite slab, reinforced with trusses, hat-shaped shear connectors, and corrugated steel plates. Tests were conducted on eight full-scale specimens subjected to transverse loads, analyzing the effects of different truss reinforcement configurations. The results showed that the variation in bending capacity due to reinforcement differences was minimal, suggesting that various configurations can be applied in large-span slabs.

The numerous attempts to combine the accessibility of prefabricated slabs with the mechanical capacity of cold-formed structures, resulted in the development of composite ribbed slabs, defined herein as ribbed floor systems in which cold-formed steel profiles are used as girders, and the space between them is filled with inert elements. During concrete casting, the steel profiles are solely responsible for bearing the construction loads, and, after this phase, the steel elements work partially or completely as rebar reinforcement. Therefore, the object of study in this research is a cold-formed steel profile coupled with a lattice girder employed in composite ribbed slabs, the so-called solution, described as follows.

1.1. *What is the Trelifácil® solution?*

The Trelifácil® solution [16] is a cold-formed steel formwork where a lattice girder is coupled by plastic spacers forming a single element, as shown in Fig. 1. This steel solution is applied to prefabricated slabs as a formwork for the ribs of the slab. Fig. 2 shows the cross-section dimensions of the CFS formwork.

1.2. *Existing investigations on the use of the Trelifácil® solution*

Although the Trelifácil® solution is already commercialised and used in the construction industry, in-depth investigations of its mechanical responses began recently. In the following, a description of the main investigations to date on the use of the Trelifácil® solution is presented.

In 2018, Favarato [17] developed a computational tool to predict the resistance capacity of flooring systems featuring this element. Later, in 2019, Favarato *et al.* [18] presented a design procedure to calculate the Trelifácil® solution as simply supported slabs without shoring during construction. In the same year, Gomes *et al.* [19] conducted four-point bending tests of simply supported beams to assess the design procedures used by Favarato *et al.* [17] to predict the moment capacity of the cold-formed steel formwork used in the Trelifácil® solution and found good agreement. In 2020, Favarato *et al.* [20] conducted studies considering the use of temporary propping during construction in the design calculations and concluded that a mean propping distance of 0.80 m must be used.

In 2022, Gomes *et al.* [21] developed a finite element model with geometric and material nonlinearity and validated it against the tests performed by Gomes *et al.* [19]. Later, Favarato *et al.* [22] presented experimental tests of full-scale prototypes of Trelifácil® solution. This research investigated the mechanical behaviour of composite slabs in terms of both strength and stiffness and concluded that the steel profile fully interacted with the concrete, increasing its bending capacity.

Finally, in 2024, Candido *et al.* [23] conducted full-scale laboratory tests to study the flexural behaviour of a composite ribbed slab employing cold-formed steel profiles as formwork before and after concrete casting. This research concluded that the trussed rebar increases the system's resistance during the construction phase. Also, the experimental data were used to propose and validate a design procedure to determine the flexural strength of the slabs during serviceability.

1.3. *Research motivation*

Due to the presence of different structural components interacting with each other, composed of materials with different properties and an

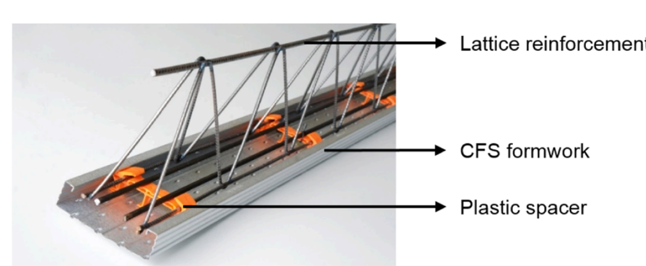

Fig. 1. Configuration of the Trelifácil® solution [16].

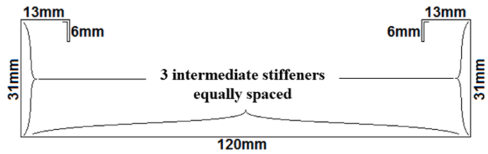

Fig. 2. Cross-section dimensions of the formwork used in the Trelifácil® solution.

unusual geometry, the analysis of composite ribbed slabs denotes a wide complexity. The usual alternative for this type of problem is the structural characterisation performed experimentally, which examines the behaviour of the system with destructive tests. On the other hand, laboratory tests do not allow the evaluation of all parameters related to the composite interaction between materials and may require expensive techniques for their set-up. An alternative to time and cost consuming experimental studies for problems of this difficulty is the use of sophisticated shell finite element analyses (SFEA), accounting for initial geometrical and physical imperfections and employing nonlinear constitutive laws. Thus, through numerical simulations validated by laboratory measurements, similarly to the concept of digital twins, it is possible to expand the empirical results and evaluate other possible parameters that allows the characterisation of the structural behaviour of composite ribbed slabs. In this matter, this research aims to show a parametric analysis to extrapolate measured data and to examine the influence of span length and cross-section thickness on the flexural capacity and stiffness of the cold-formed profile used in the Trelifácil® solution. The following sections describe the research methodology and results for the parametric analysis.

2. Methodologies

This section presents the validated finite element model used to perform the parametric analysis and the considerations used in the theoretical predictions.

2.1. Testing program

2.1.1. Cold-formed profile – testing setup

The validated finite element model developed by Gomes *et al.* [21] was used in this research to perform the parametric analysis. The numerical model was validated against experimental data from four-point bending tests. Two groups of three specimens were tested which were designated according to their free span length. The shorter profiles (designated as P0.5 in numerical analyses) received the labels P0.5a, P0.5b and P0.5c and have a free span length of 0.5 m. The 0.90 m beams (designed as P0.9 in numerical analyses) were identified as P0.9a, P0.9b and P0.9c. The specimens were tested about the minor axis of inertia (lips under compression), as used in their final application. Fig. 3 shows the test setup. The measured data is reported through peak loads P_u and ultimate bending moments M_u, as presented in Table 1.

2.1.2. Trelifácil® solution entire configuration – testing setup

Experimental data of four-point bending tests conducted by Candido *et al.* [23] was used to validate the numerical models of the entire configuration of the Trelifácil® solution, i.e., a trussed girder attached to a cold-formed steel member. This section presents the main testing features and results.

Four groups of two specimens were used in this work to validate the numerical models. They were designated according to their free span length (1.0 m, 1.4 m and 1.8 m) and the trussed girder height (16 cm and 12 cm). They were designated as PST1.0_16, PST1.4_16, PST1.8_16 and PST1.8_12. Geometrical properties were taken from Candido *et al.* [23], as well as material properties that were obtained from material tests. Fig. 4 shows the testing setup parameters and Table 2 its respective values. Fig. 5 presents the Trelifácil entire configuration testing setup [23]. Results are displayed in Fig. 6 in terms of load *versus* displacement.

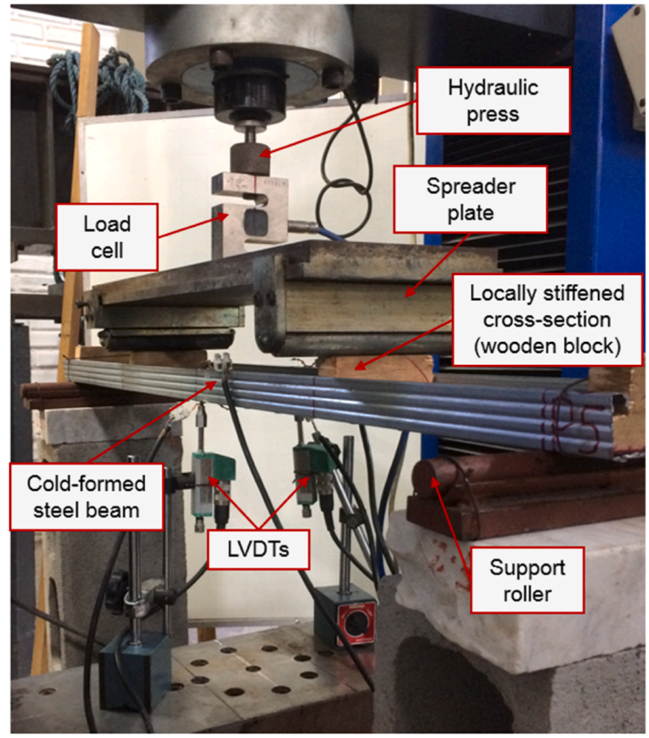

Fig. 3. Experimental layout of four-point bending tests [21].

2.2. Finite element model validation

2.2.1. Cold-formed profile – numerical validation

The finite element results are obtained with the modelling techniques used by Gomes *et al.* [21]. ANSYS finite element package [24] was used to perform the analysis. The finite element mesh has four-node shell elements (SHELL181) with nominal mesh size of 4 mm and 21 points of integration through the cross-section thickness and no initial geometrical imperfections. Loads were applied with displacement control. Full Newton-Raphson method controlled by artificial damping was used to perform the geometrical and material nonlinear analyses.

A plasticity model represented by a multilinear stress-strain curve with von Mises yield criterion, associative flow rule and isotropic hardening were used to represent the material. The basic Ramberg-Osgood stress-strain relationship up to 0.2 % proof stress followed by a straight line with a constant slope expressed as a fraction of initial elastic modulus ($E = 200\ GPa$), as shown in Eq. (1). The value of $E/50$ was adopted for the slope of the straight line and the shape parameter n equal to 28, as in Haidarali and Nethercot [25] and Ye *et al.* [26].

An elastic modulus of 200 GPa was adopted and yield stress (0.2 % proof stress, $\sigma_{0.2}$) of 290 MPa provided by the steel manufacturer laboratory tests was used. Additionally, large-strain analyses (NLGEOM,ON) are performed in this study, then all the input engineering values for stresses and strains in the large-strain region (i.e., after 0.2 % proof stress) are converted to true values. Fig. 7 illustrates the material curve.

$$\begin{aligned} \epsilon_e &= \frac{\sigma_e}{E} + 0,002\left(\frac{\sigma_e}{\sigma_{0,2}}\right)^n \qquad for\ \sigma \le \sigma_{0,2} \\ \epsilon_e &= \epsilon_{0.2} + \frac{50(\sigma - \sigma_{0,2})}{E} \qquad for\ \sigma > \sigma_{0,2} \end{aligned} \tag{1}$$

To assess the model's sensitivity to element choice and mesh density, different element types and sizes were investigated. The four-node and eight-node shell elements SHELL181 and SHELL281, respectively, both

Table 1
Summary of the experimental tests results from Gomes *et al.* [21].

Photos	Specimen	Span length (m)	P_u (kN)	M_u (kN.m)
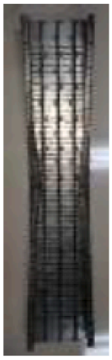 	Specimen P0.5a	0.50	4.16	0.26
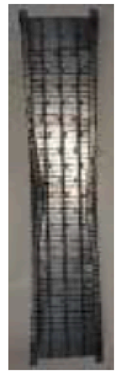 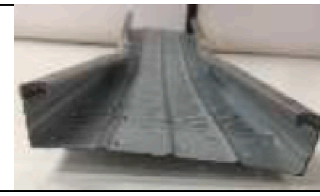	Specimen P0.5b	0.50	4.06	0.25
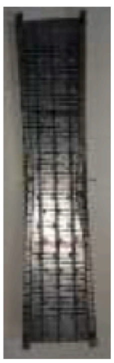 	Specimen P0.5c	0.50	4.30	0.27
 	Specimen P0.9a	0.90	2.55	0.29
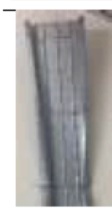 	Specimen P0.9b	0.90	2.38	0.27
 	Specimen P0.9c	0.90	2.29	0.26

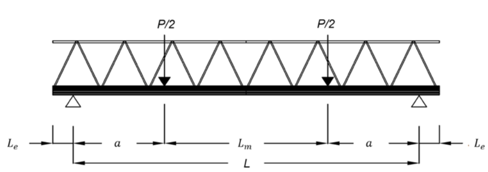

Fig. 4. testing setup parameters of Candido *et al.* [23].

Table 2
Longitudinal dimensions of the prototypes used by Candido *et al.* [23].

Prototype	L (mm)	Le (mm)	L_m (mm)
PST1.0_16a	100	10	464.25
PST1.0_16b	100	10	464.25
PST1.4_16a	140	10	464.25
PST1.4_16b	140	10	464.25
PST1.8_16a	180	9.95	464.25
PST1.8_16b	180	9.8	464.25
PST1.8_12a	180	9.75	464.25
PST1.8_12b	180	9.75	464.25

with six degrees-of-freedom (DOF) at each node, were analysed. A mesh study was performed with nominal element size varying from 100 mm to 3.5 mm with an aspect ratio, i.e., plate's length-to-width ratio, equal to one for flat elements, so that it is close to five for corner elements.

The following modelling techniques were used in the studies: multilinear material model, loading with displacement control, Full Newton-Raphson solver solution method controlled by artificial damping and no initial geometric imperfections. In addition, a cross-section thickness of 0.52 mm and beam free span length of 0.9 m were used in all analyses presented in this section. Also, default element options (KEYOPT) were used for both shell models and no issues related to shear locking were observed. Thereby, appropriate element type and mesh density could be selected for future finite element models.

Fig. 8 shows the ultimate bending moment *versus* number of elements for models with SHELL181 and SHELL281 elements. Both shell models presented rapidly convergent solutions. Thus, all subsequent analyses are performed with 4 mm mesh size, i.e., 33.000 elements, since the ultimate bending moment deviated only 0.1 % from results obtained with the finer mesh model. SHELL181 element was selected for subsequent analyses, since neither computational cost nor response accuracy

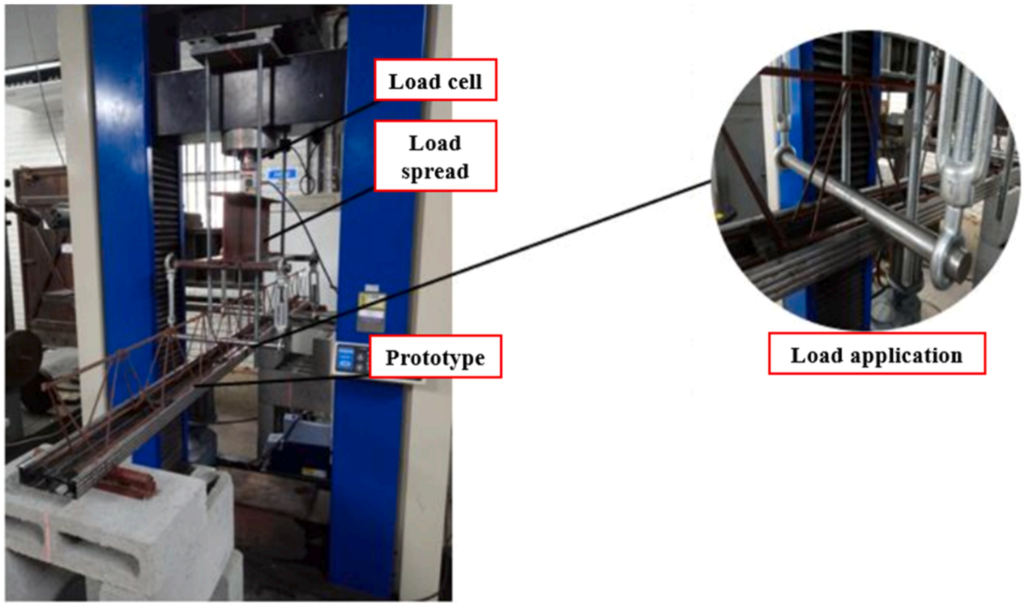

Fig. 5. Trelifácil® entire configuration testing setup of Candido *et al.* [23].

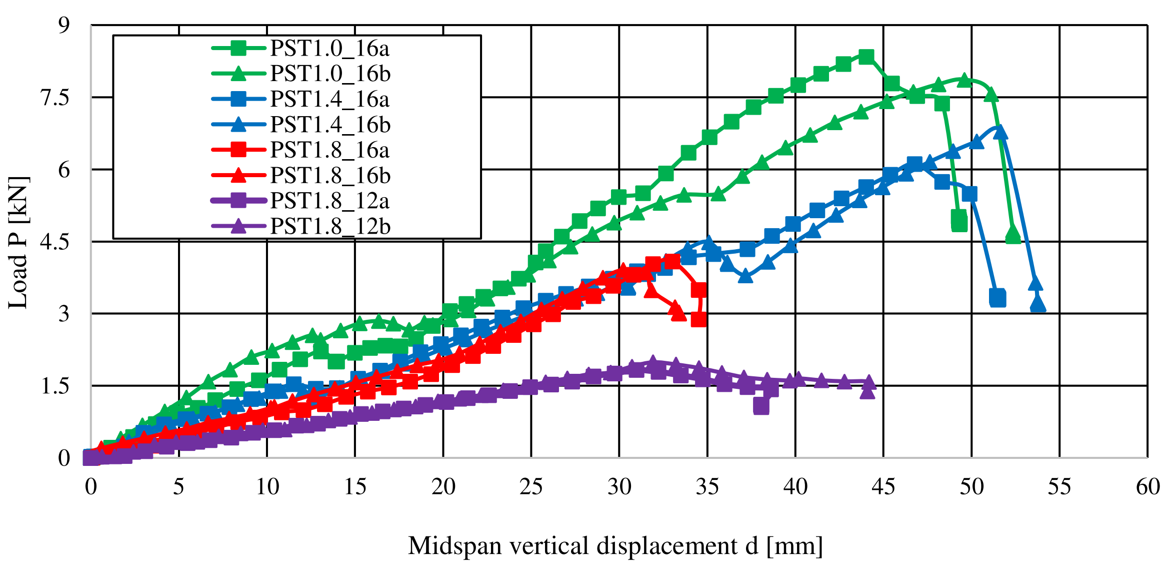

Fig. 6. Trelifácil® entire configuration testing results in terms of load *versus* displacement found by Candido *et al.* [23].

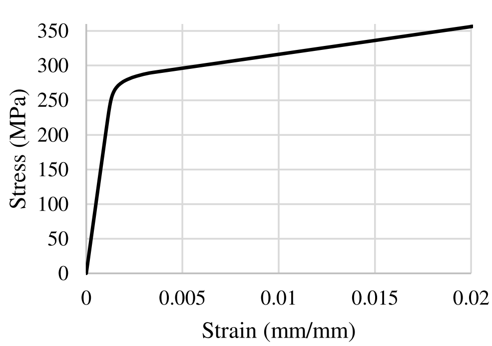

Fig. 7. Plasticity model represented by a multilinear stress-strain curve.

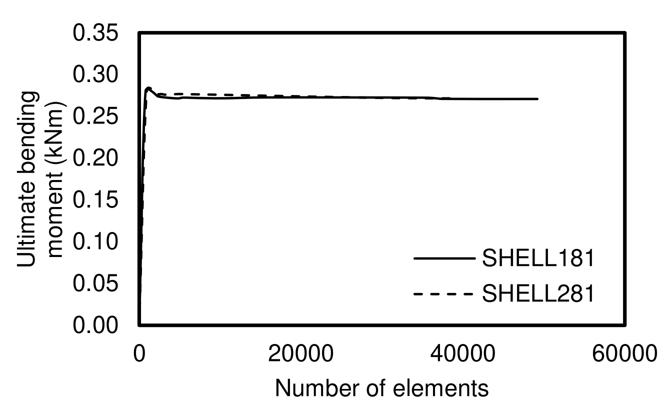

Fig. 8. Ultimate bending moment *versus* number of SHELL181 and SHELL281 elements.

were improved with the use of SHELL281 elements.

Fig. 9 illustrates the number of elements used to represent the main portions of the beams cross-section. Overall, 116 nodes are used to

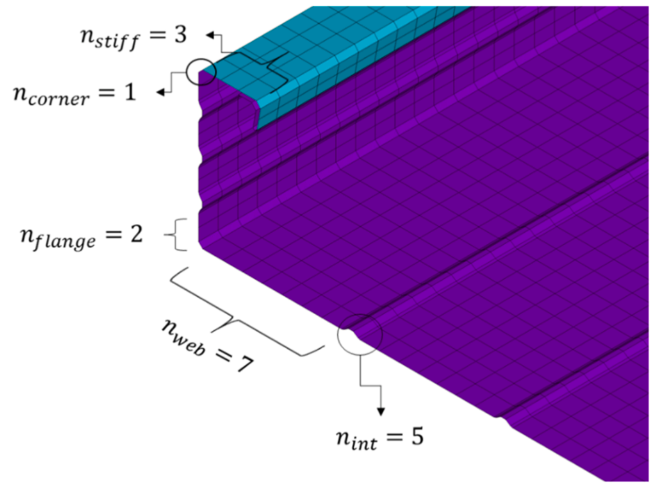

Fig. 9. Illustration of the number of elements used to represent the main portions of the beams cross-section.

discretize the member cross-section, corresponding to: three elements for stiffeners (n_{stiff}), one element for corners (n_{corner}), two elements for flat flange portions (n_{flange}), seven elements for flat web portions(n_{web}) and five elements for intermediate stiffeners (n_{int}).

In this research no geometrical imperfections were applied since they demonstrated to have low impact in the ultimate bending moment. Fig. 10 shows the load-displacement responses of the nonlinear analysis conducted with different initial geometrical imperfection factors. Such imperfections were applied from imperfection shapes obtained from finite element buckling modes factored by 0.1t, 1.0t and 4.0t, where t is the member thickness.

Finally, Table 3 presents the finite element moment capacity $M_{u,FE}$ normalised by experimental values $M_{u,Exp}$ in the context of comparisons between finite element and experimental flexural strength responses. A mean $M_{u,FE}/M_{u,exp}$ ratio of 1.03 was obtained demonstrating their good agreement. Other results such as load-displacement curve and collapse modes can be assessed in Gomes *et al.* [21].

2.2.2. *Trelifácil® solution entire configuration – numerical model*

2.2.2.1. Modelling techniques for Trelifácil® entire configuration. The following section describe the basic features of the finite element model developed for the Trelifácil® solution entire configuration, that is: boundary condition and loading position, mesh and element discretization, material models, initial geometrical imperfections and solution scheme.

A finite element mesh of 4 mm linear shell elements with reduced integration (SHELL181) is used to represent the CFS member. A multi-linear isotropic hardening material model was used to model the stress-strain behaviour of the steel formworks. Moreover, Full Newton-Raphson method solution scheme with nonlinear stabilisation (STABILIZE) was employed to solve the nonlinear analyses for the model of trussed girder coupled to the CFS member. In what follows, a brief description of the finite modelling techniques implemented to include the trussed girder in the finite element model developed for the cold-formed steel member is presented.

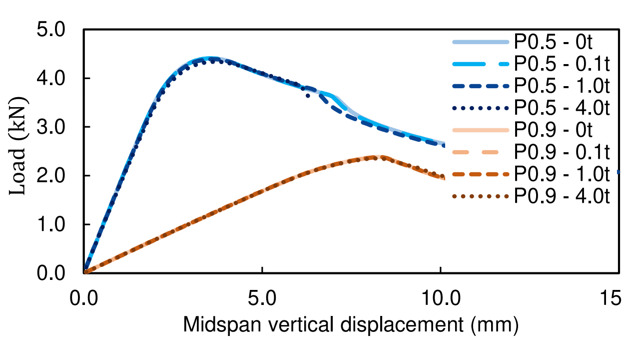

Fig. 10. Load-displacement responses of the initial geometrical imperfection sensitivity study with different magnitude factors.

Table 3
Comparison of finite element strength and stiffness predictions with average experimental results [21].

Specimen	$M_{u,FE}/M_{u,exp}$
P0.5a	1.06
P0.5b	1.09
P0.5c	1.03
P0.9a	0.94
P0.9b	1.01
P0.9c	1.05
Average	**1.03**
Coefficient of variation (COV)	**0.04**

Beam elements with six degree of freedom (BEAM188) at each node are used to discretise geometry of the trussed girder. In this research, BEAM188 elements with linear shape function are used. The finite element mesh is created with 11 elements for diagonal chords and 22 elements for top and bottom chords between connection points. An elastic perfectly-plastic material model is implemented to simulate the trussed girder steel stress-strain behaviour. Material properties are adopted in accordance with material tests presented in Candido *et al.* [23].

2.2.2.2. Study of the interaction between the trussed reinforcement and the cold-formed steel member. The trussed girder and cold-formed steel formwork are connected to each other via plastic spacers. As an alternative for modelling plastic spacers, the strategy employed herein to simulate their influence on the structural system was to couple the degrees of freedom (DOF) of nodes positioned near the connected region. As shown in Fig. 11, the bottom chords of the trussed girder are fixed on the plastic spacers, which in turn are fixed on the steel formwork. It is expected that vertical displacements (UY) can be transferred from the nodes on the web of the steel member to nodes along the bottom chord of the trussed girder. Similarly, horizontal displacements in the transversal direction (UX) can be linked between nodes of bottom chords and the steel member flange, where the plastic spacers are fixed. Therefore, the study described in this section aims to present the finite element model sensitivity to the amount of coupled DOF. To this end, nonlinear analyses are conducted and compared with experimental data to investigate two different aspects:

a) whether to (i) exclude or (ii) include compatibility of the rotational degrees of freedom (ROTZ and ROTX) between nodes of the trussed girder and formwork in regions connected by plastic spacers;
b) consideration of (iii) full or (i and ii) no interaction of translations in the longitudinal direction (UZ) promoted by the plastic spacers.

Fig. 12 shows the boundary conditions, loading position and sets of coupled DOF applied to the sensitivity studies of the Trelifácil® solution finite element model. Nine sets of coupled DOF are applied at distances of 150 mm along the length of the CFS member. Although the manufacturer recommends a distance of 330 mm between plastic spacers, shorter spacing was applied to promote more interaction between the components of the Trelifácil® solution. In addition, Fig. 12 presents the FE model with only transversal DOF couples (i.e., UX and UY) in the region of the plastic spacers, which corresponds to investigation (i). On the second case, labelled as (ii), rotations about X and Z axis (ROTX and ROTZ) are coupled and boundary conditions are identical to case (i), as shown in Fig. 12. Alternatively, on case (iii) the boundary conditions are

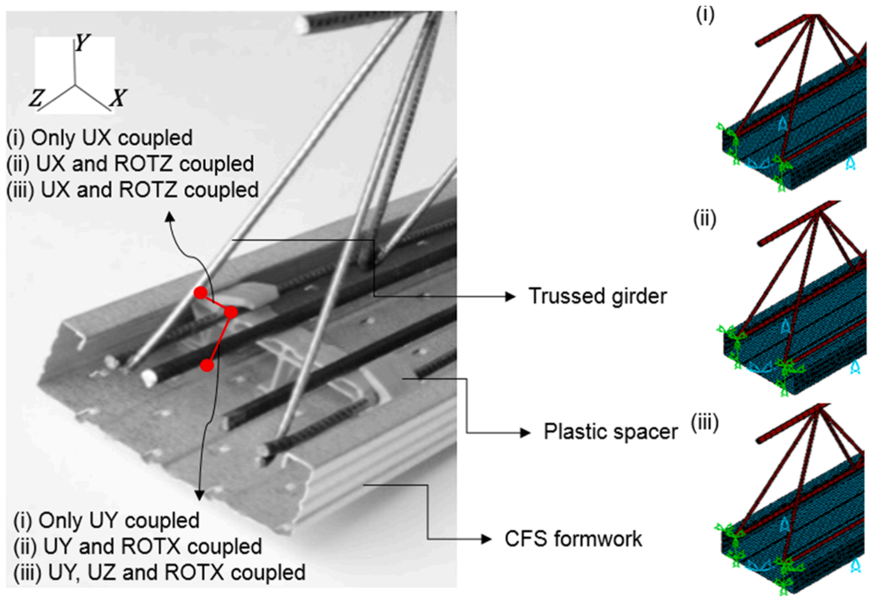

Fig. 11. Illustration of three possible node coupling to assess the interaction between trussed girder and CFS formwork provided by plastic spacers.

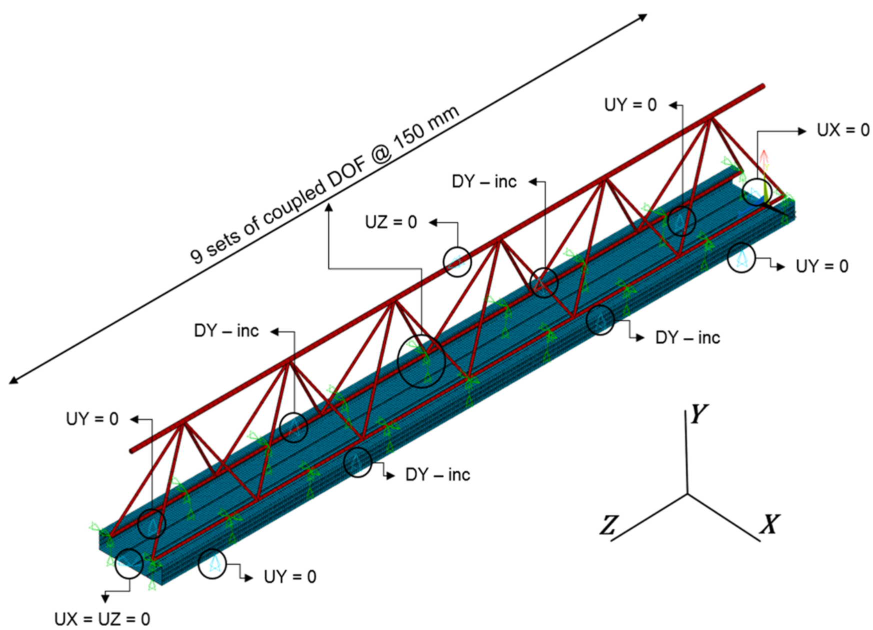

Fig. 12. Boundary conditions, loading position and sets of coupled degrees-of-freedom (DOF) applied to the sensitivity studies of the Trelifácil® solution finite element model.

slightly changed. Since the longitudinal displacements are coupled between trussed girder and CFS member nodes, the imposed restraint in the Z-direction applied to the node on the top chord at midspan is removed. This restraint was originally applied to prevent the trussed girder from undergoing rigid body motion in the finite element models of the cases (i) and (ii).

The load-displacement responses of the finite element models are shown in Fig. 13. It was observed that the composite action between cold-formed steel beam and trussed girder was more sensitive to the connection of longitudinal displacements (UZ) than rotational DOF (ROTX and ROTZ). A quantitative analysis can be carried out using Fig. 14, where the ultimate moment capacity $M_{u,FE}$ and stiffness $(EI)_{FE}$ of cases (ii) and (iii) are normalised by the ultimate moment capacity $M_{u,FE,i}$ and stiffness $(EI)_{FE,i}$ of case (i), i.e., an equivalent system without coupling the longitudinal displacements (UZ) and rotational degrees-of-freedom (ROTX and ROTZ). Whereas the flexural capacity and stiffness of the FE model (iii) increased more than 50 % relative to case (i), these gains were below 10 % for case (ii).

2.2.2.3. Validation model for the Trelifácil® entire configuration. Fig. 15 compares experimental and numerical data through the load *versus* displacement curves for the four prototype groups analyzed. The comparison utilizes case (i) of node coupling, where only the UX degree of freedom—without longitudinal or rotational coupling—was applied between the truss girder and the cold-formed profile.

The validation of the numerical model was carried out focusing on the portion of the load-displacement curve that precedes the maximum displacement allowed for compliance with the Serviceability Limit States (SLS), as established by the Brazilian standard ABNT NBR 14762:2010 [25], which governs the design of structures made from

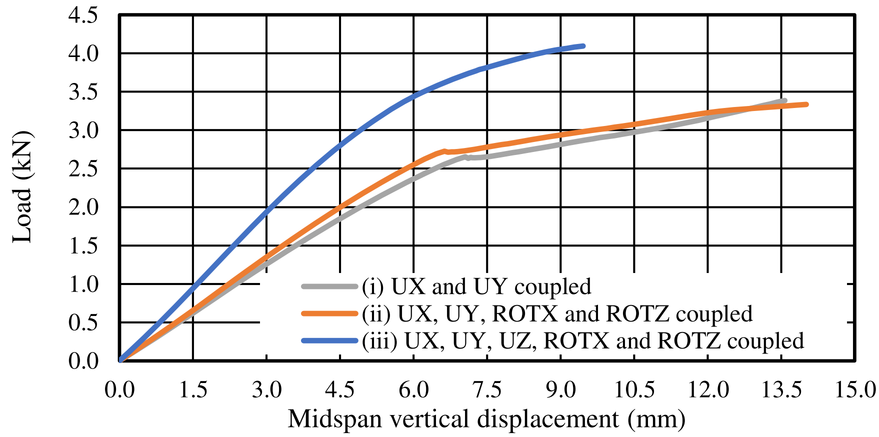

Fig. 13. Force *versus* displacement curves of the FE models (i), (ii) and (iii).

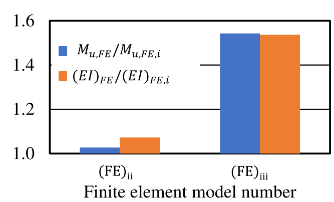

Fig. 14. Enhancements in moment capacity and flexural stiffness of the FE model (ii) and model (ii) relative to the FE model (i).

cold-formed steel profiles.

According to this standard, the allowable displacement limit for SLS verification is L/350, where L is the span between supports. It was observed that, in the tests performed, the load corresponding to the onset of structural collapse (characterized by the "drop" in the load-displacement curve) occurs after the maximum displacement allowed by the standard has been exceeded.

Therefore, the comparison between experimental and numerical results was based on the load corresponding to the displacement limit of L/350, since this is the normative criterion applicable to ensure the in-service performance of the structure. The decision to validate the model within this region of the curve is justified by its more accurate representation of structural behavior within the usage limits prescribed by the standard, ensuring compliance with the performance and safety requirements established for the SLS.

For validation purposes, only the groups with spans of 1.4 m and 1.8 m were considered. This decision is based on the findings of Candido *et al.* [23], who reported that the collapse of the 1.0 m span group occurred at the supports rather than within the flexural span. Since the primary objective of this study is to evaluate the flexural behavior of the members, the results from the 1.0 m span group were excluded from the analysis. Table 4 presents a comparison between the finite element predictions and the average experimental results for the serviceability limit state (SLS) load of the complete Trelifácil® system. The numerical and experimental results showed good agreement, with a mean ratio of 0.96.

2.3. Theoretical predictions of the cold-formed profile

The Direct Strength Method presented in the Brazilian standard ABNT NBR 14762:2010 [27] is used to obtain the theoretical predictions of nominal flexural strength ($M_{Rk,DSM}$) evaluated in this research. The finite strip software CUFSM [28,29] is used to determine the local and distortional critical buckling moments for the examined cross-section, as shown in Fig. 16. Table 5 presents the values of critical buckling moments, slenderness and moment capacity for specimens P0.5 and P0.9. Mean values of thickness (0.52 mm) and yield stress (290 MPa) provided by the manufacturer were used to perform the stability analysis. In both cases, distortional buckling controlled the moment capacity predictions.

2.4. Parametric analysis techniques – cold-formed profile

The finite element models developed herein were validated against physical tests that follows the recommendations of full cross-section bending tests prescribed by the European code for cold-formed steel structures EN 1993-1-3:2004 [30]. This code establishes that “a pair of point loads should be applied to the specimen to produce a length under uniform bending moment at midspan of at least 0.2 x (span) but not more than 0.33 x (span)”. In the experimental program, however, the distance between loading points were set equal to 0.46425 m for all tests. Therefore, this distance was altered to 0.33 x (span) for all numerical models of the parametric studies. Furthermore, to prevent rigid body motion, transversal horizontal displacements (U_x) are restrained at both ends and longitudinal displacements (U_z) at one end. Fig. 17 shows an overall view of the boundary conditions and loading position used in these parametric studies. The remaining features of the finite element model are equal to those adopted in the validated model.

2.5. Parametric analysis techniques – Trelifácil® entire configuration

The modelling techniques implemented here were similar to those described in section 2.4 for the cold-formed steel member. Conservatively, it is assumed for the degree of coupled action between the Trelifácil® solution components that no longitudinal displacements (UZ) and rotational DOF (ROTX and ROTZ) are transferred by the plastic spacers. The remaining features of the finite element model are equal to those adopted in the validated model.

3. Results

3.1. Evaluated parameters for the cold-formed profile

The parametric studies presented herein aimed to assess the influence of different span lengths and section thicknesses on the ultimate bending moment $M_{u,FE}$. In addition, these results are used to examine the accuracy of the nominal resistant bending moment calculated with the Direct Strength Method (M_{DSM}).

The nominal resistant bending moment calculated with the DSM ($M_{u,DSM}$) relies on the determination of critical elastic moments related to flexural-torsional buckling (M_e), local buckling (M_ℓ) and distortional buckling (M_{dist}). In this research, those values are taken from the findings of Favarato *et al.* [18] which were determined using finite element buckling analysis and are shown in Table 6. To assess the accuracy of

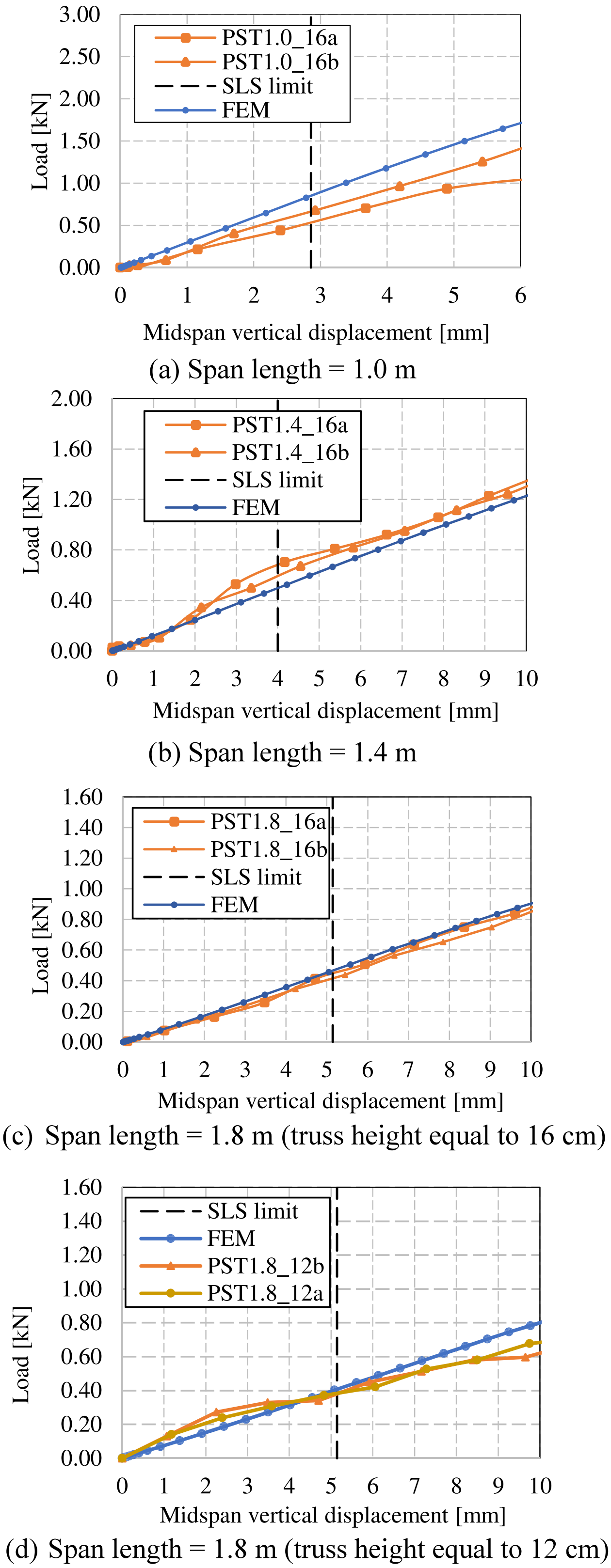

Fig. 15. Confrontation of the load-displacement response obtained from the finite element analysis and experimental tests of Candido *et al.* [23].

those values, critical elastic moments related to local and distortional buckling were also obtained using CUFSM [26,27] and good agreement was found between finite element and finite strip buckling moments. As such, the values from Favarato *et al.* [18] were used in the parametric studies to maintain the consistency with these previous studies.

Table 4
Comparison of finite element with average experimental results of load at SLS limit for the Trelifácil® entire solution.

Specimen	$F_{SLS,FE}/F_{SLS,exp}$
PST1.4_16a	0.71
PST1.4_16b	0.81
PST1.8_16a	1.04
PST1.8_16b	1.12
PST1.8_12a	1.06
PST1.8_12b	1.07
Average	**0.96**
Coefficient of variation (COV)	**0.15**

Table 6 presents values of critical buckling moments for cold-formed steel members with eight different free span lengths (L), varying from 0.6 m to 2 m, for three different cross-sectional thicknesses, 0.65 mm, 0.8 mm, and 1.08 mm. Thickness values greater than the nominal thickness (i.e., 0.65 mm) are used to evaluate the sensitivity of the flexural behaviour to changes in cross-sectional dimensions. Therefore, a total of 24 beams are tested in this parametric study.

3.2. Results and discussion for the cold-formed profile

Fig. 18. This graph shows the influence of free span length and cross-section thickness on moment capacity of the Trelifácil® CFS member. Overall, the moment capacity was higher for members with thicker cross-sections, and it rises more gradually for smaller cross-section thicknesses. Further, for all cross-section thicknesses assessed, this value tends to remain unaltered for longer span lengths.

Table 7 and Fig. 19 show the parametric studies in the context of comparisons between theoretical (DSM) and finite element predictions of moment capacity.

In general, the DSM presented conservative results. Closer agreement between theoretical and numerical results was found for longer spans thicker cross-sections. For shorter spans the results appear to present greater divergence between results. As expected, the flexural strength according to DSM tends to increase for smaller spans. However, in numerical analyses, the opposite happens. with a decrease in flexural strength. Regarding this point, it is important to highlight that finite element models simulate four-point bending. Therefore, the results can be influenced by limit states associated with load point crippling and combined shear and bending. However, this study scope was limited to the bending moment. In future investigations, other collapse modes and their correlations with theoretical predictions can be evaluated.

3.3. Evaluated parameters for the Trelifácil® entire configuration

A series of parametric studies is conducted to investigate the influence of trussed girder on the flexural stiffness of the structural member. Similar evaluated parameters of spans, thicknesses, boundary conditions and load application from the parametric analysis presented for the cold-formed steel member, as presented in Section 3.1. Trussed girder types with height of 160 mm (TR16745) was selected. Results were analysed in terms of gains in the flexural strength at the maximum displacement for service limit state requirements of ABNT NBR 14762:2010 [27] Brazilian code. Results are presented in the following section.

3.4. Results and discussion for the Trelifácil® entire configuration

Enhancement in flexural strength of the Trelifácil® solution is assessed through the results of twenty-four nonlinear analyses of the entire system and comparisons with corresponding CFS member without trussed girder included. Table 8 presents the results of parametric studies in terms of gains in flexural strength at SLS maximum displacement (L/350) due to the trussed rebar addition. Fig. 20

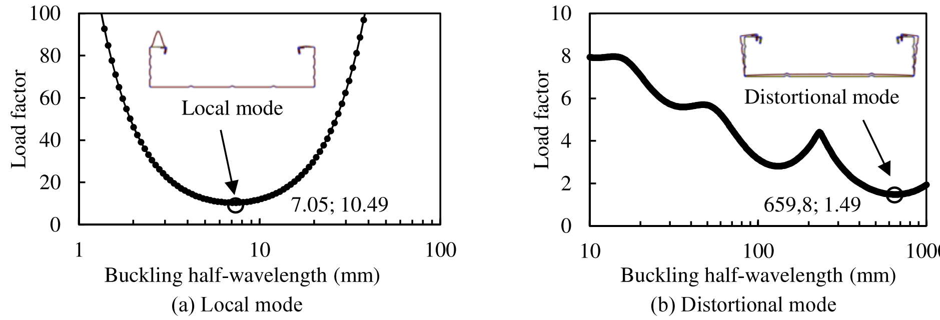

Fig. 16. Signature curve from CUFSM [26,27] for typical examined cross-section.

Table 5
Theoretical predictions of nominal flexural strength (in kNm) per Direct Strength Method for the specimens of the pilot experimental program.

		Lateral-torsional buckling			Local buckling			Distortional buckling			$M_{Rk,DSM}$
	Wf_y	M_e	l_0	$M_{R,e}$	M_ℓ	l_ℓ	$M_{R,\ell}$	M_{dist}	l_{dist}	$M_{R,dist}$	
P0.5	0.27	10.22	0.16	0.27	2.86	0.31	0.27	0.39	0.83	0.24	0.24
P0.9	0.27	3.17	0.29	0.27	2.86	0.31	0.27	0.39	0.83	0.24	0.24

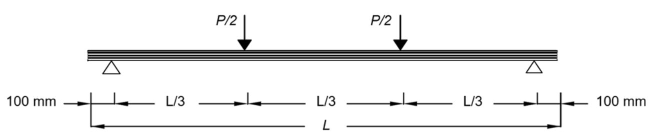

Fig. 17. Boundary condition and loading position used in the parametric studies.

illustrates such results.

Based on the analysis of Fig. 20, it is observed that the Trelifácil® system — composed of a steel profile combined with a truss — exhibits significantly superior flexural performance compared to the isolated steel profile. For all thicknesses evaluated (0.65 mm, 0.8 mm, and 1.08 mm), the results indicate substantial gains in flexural strength when the truss acts in conjunction with the profile.

These gains become more pronounced as the span of the model increases. For shorter spans, such as 0.5 m and 1.0 m, the increases range approximately between 20 % and 80 %, depending on the profile

Table 6
Critical buckling moments (in Nm) for the Trelifácil® solution cold-formed steel beam with different free span lengths and cross-sectional thicknesses.

L (m)	t = **0.65 mm**			t = **0.8 mm**			t = **1.08 mm**		
	M_e	M_ℓ	M_{dist}	M_e	M_ℓ	M_{dist}	M_e	M_ℓ	M_{dist}
0.6	1151.7	1147.4	575.7	1498.2	1779.3	909.9	2034.3	3339.7	1792.0
0.8	1083.7	1147.7	645.9	1407.8	1755.0	967.3	1919.0	3295.8	1653.2
1	911.2	1180.8	598.7	1204.6	1742.0	899.8	1632.6	3280.7	1664.8
1.2	613.4	1154.9	588.4	870.6	1734.5	931.6	1287.5	3274.9	1661.5
1.4	537.2	1145.2	618.2	721.4	1730.2	912.8	1007.3	3270.5	1645.4
1.6	451.2	1147.0	591.8	588.1	1727.4	905.9	802.1	3266.3	1667.8
1.8	375.4	1115.1	590.5	482.8	1725.8	926.1	652.9	3264.4	1647.3
2	314.1	1113.9	604.5	401.9	1724.5	908.7	542.7	3263.3	1680.7
CUFSM	–	1117.1	612.9	–	1825.1	941.3	–	3486.3	1755.3

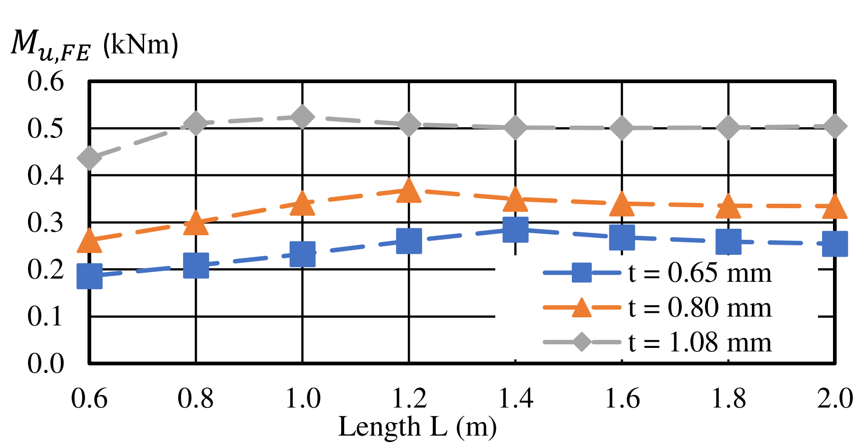

Fig. 18. Influence of free span length and cross-section thickness on moment capacity of the Trelifácil® CFS member.

Table 7
Results of parametric studies in terms of moment capacity.

L	t = 0.65 mm			t = 0.80 mm			t = 1.08 mm		
	$M_{u,FE}$	M_{DSM}	$\frac{M_{DSM}}{M_{u,FE}}$	$M_{u,FE}$	M_{DSM}	$\frac{M_{DSM}}{M_{u,FE}}$	$M_{u,FE}$	M_{DSM}	$\frac{M_{DSM}}{M_{u,FE}}$
(m)	(kNm)	(kNm)		(kNm)	(kNm)		(kNm)	(kNm)	
0.6	0.19	0.34	1.83	0.26	0.45	1.72	0.44	0.63	1.45
0.8	0.21	0.35	1.70	0.30	0.46	1.53	0.51	0.63	1.24
1.0	0.23	0.35	1.48	0.34	0.45	1.22	0.52	0.63	1.19
1.2	0.26	0.34	1.32	0.37	0.44	1.26	0.51	0.60	1.19
1.4	0.28	0.34	1.19	0.35	0.43	1.25	0.50	0.58	1.15
1.6	0.27	0.32	1.21	0.34	0.40	1.20	0.50	0.55	1.09
1.8	0.26	0.30	1.17	0.34	0.38	1.13	0.50	0.51	1.02
2.0	0.25	0.28	1.10	0.33	0.35	1.05	0.50	0.47	0.94
Mean			1.37			1.30			1.16
Standard deviation			0.22			0.17			0.11

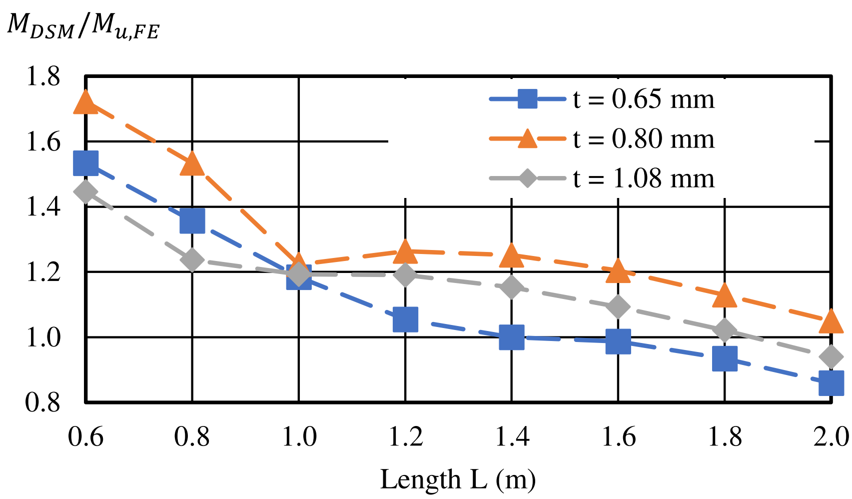

Fig. 19. Comparison of the flexural capacity and midspan vertical deflection obtained from DSM and FE analysis.

Table 8
Results of parametric studies in terms of gains in flexural strength at SLS maximum displacement ($\boldsymbol{L}/350$) due to the trussed rebar addition.

L	t = 0.65 mm			t = 0.80 mm			t = 1.08 mm		
	F_{SLS_P}	F_{SLS_PST}	$\frac{F_{SLS\_PST}}{F_{SLS\_P}}$	F_{SLS_P}	F_{SLS_PST}	$\frac{F_{SLS\_PST}}{F_{SLS\_P}}$	F_{SLS_P}	F_{SLS_PST}	$\frac{F_{SLS\_PST}}{F_{SLS\_P}}$
(m)	(mm)	(mm)		(mm)	(mm)		(mm)	(mm)	
0.6	1.18	1.52	28.1 % %	1.58	1.96	24.2 %	2.39	2.79	16.8 %
0.8	0.79	1.42	80.5 %	1.05	1.89	79.2 %	1.57	2.73	74.1 %
1.0	0.58	0.90	56.0 %	0.76	1.13	48.2 %	1.10	1.51	37.1 %
1.2	0.44	0.75	71.0 %	0.57	0.94	65.2 %	0.81	1.26	56.5 %
1.4	0.34	0.60	75.3 %	0.44	0.73	67.7 %	0.61	0.95	55.8 %
1.6	0.27	0.81	196.7 %	0.34	1.07	211.4 %	0.47	1.54	224.4 %
1.8	0.22	0.63	183.0 %	0.28	0.79	186.7 %	0.38	1.07	184.2 %
2.0	0.18	0.56	210.7 %	0.23	0.71	212.3 %	0.31	0.94	205.8 %

thickness. Within this range, there is a slight tendency for thinner profiles — especially the 0.65 mm one — to show slightly higher gains compared to thicker profiles. This behaviour may be related to the relatively greater efficiency of the truss's contribution in thinner profiles.

On the other hand, for longer spans, between 1.5 m and 2.0 m, there is a significant increase in flexural strength gains, reaching values close to or exceeding 200 %. In this range, the curves corresponding to the different thicknesses become quite close, indicating that for longer spans, the influence of the steel profile thickness on the gains provided by the combined system is less significant.

This analysis reinforces the importance of considering the Trelifácil system — with the steel profile and truss acting integrally — already in the pre-concrete curing phase. This approach allows for better exploitation of the system's structural potential, enabling the design of slabs with longer spans without the need for temporary propping.

4. Conclusion

Finally, two validated finite element models are presented to develop parametric studies to examine the structural performance of the Trelifácil® solution in the construction phase. In addition, the accuracy of the Direct Strength Method to predict the flexural strength of the cold-formed steel member about the minor axis of inertia was assessed for different span lengths and cross-section thicknesses.

The main conclusions from the parametric analysis are that the

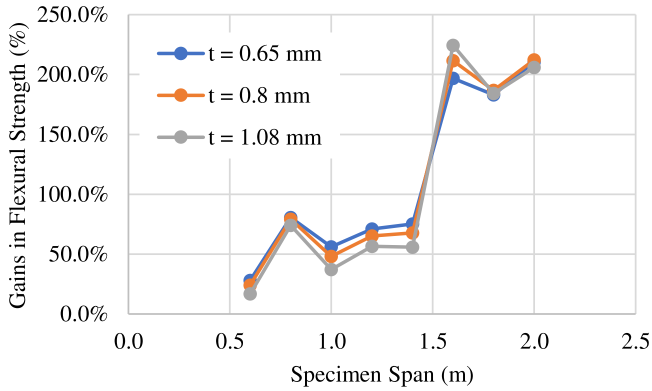

Fig. 20. Enhancements in flexural strength at SLS maximum displacement (*L* /350) of the Trelifácil® solution relative to the corresponding CFS member without trussed girder included.

moment capacity of the cold-formed steel beams tends to plateau with the increase of span length, and it increases for thicker material. When DSM predictions of bending moment were compared with finite element results conservative results were found. In general, the DSM has proven to be an acceptable methodology to supply the ultimate bending moment for the structural design of the Trelifácil® solution during the construction phase.

However, some finite element results presented high discrepancy with the DSM predictions. These results can highlight potential areas of future research using numerical analysis, such as the investigations on loading point crippling and combined shear and strength. This would provide support to carry out robust studies on the behaviour of these beams under loading and boundary conditions as used in service or even under extreme loads. Continuous beams under uniformly distributed loading would represent, for instance, a real condition of the system, which involves the use of propping to support the slab until it gains enough strength to support itself.

Finally, a numerical model was developed to simulate the composite action between the cold-formed profile and the attached trussed girder for the entire configuration of the Trelifácil® solution. Numerical results were confronted with experimental data showing that the no longitudinal translation and any rotation is transferred promoted by the plastic spacers.

Moreover, parametric analysis demonstrated that the Trelifácil system, combining a steel profile with a truss, significantly enhances flexural performance compared to the isolated profile. This improvement is evident across all tested thicknesses and becomes more pronounced with increasing span lengths, reaching gains of over 200 % for spans between 1.5 m and 2.0 m. These findings highlight the structural efficiency of the integrated system, particularly in longer spans, and reinforce the importance of considering this configuration from the pre-concrete curing phase to enable slab designs without temporary propping.

Author Statement

We, the undersigned authors, hereby declare that the manuscript titled "Parametric Study of a Cold-Formed Steel Profile Employed in Composite Ribbed Slabs" is an original work and has not been submitted or published elsewhere in any form.

CRediT authorship contribution statement

André V.S. Gomes: Writing – review & editing, Software, Formal analysis, Writing – original draft, Methodology, Conceptualization, Validation, Investigation. **Daniel C.M. Candido:** Methodology, Writing – review & editing, Investigation, Validation, Formal analysis. **Lucas F. Favarato:** Validation, Formal analysis, Methodology, Writing – review & editing, Investigation. **Johann A. Ferrareto:** Supervision, Resources, Writing – review & editing. **Juliana C. Vianna:** Supervision, Resources, Writing – review & editing. **Adenilcia F.G. Calenzani:** Supervision, Resources, Writing – review & editing.

Declaration of competing interest

The authors declare that they have no known competing financial interests or personal relationships that could have appeared to influence the work reported in this paper.

Acknowledgements

The authors express their gratitude to ARCELORMITTAL BRASIL S.A and the Brazilian Government Agencies FAPES and CAPES for their financial support during this research. The last author also extend thanks to the Brazilian Government Agency FAPES for the research productivity grant.

Data availability

The data that has been used is confidential.

References

[1] S. Torabian, B. Zheng, B. Schafer, Experimental study and modeling of cold-formed steel lipped channel stub beam-columns, in: *Proceedings of the Structural Stability Research Council Annual Stability Conference* 2014, 2014. *SSRC 2014*.
[2] S. Torabian, B. Zheng, B.W. Schafer, Experimental response of cold-formed steel lipped channel beam-columns, Thin-Walled Struct. 89 (2015) 152–168.
[3] H. Wang, Y. Zhang, Experimental and numerical investigation on cold-formed steel C-section flexural members, J. Constr. Steel Res. 65 (5) (2009) 1225–1235.
[4] American Iron and Steel Institute (AISI), North American specification for the design of cold-formed steel structural members, AISI S100-12, Washington, D.C., 2012.
[5] N. Kumar, D.R. Sahoo, Optimization of lip length and aspect ratio of thin channel sections under minor axes bending, Thin-Walled Struct. 100 (2016) 158–169.
[6] B.W. Schafer, Review: the direct strength method of cold-formed steel member design, J. Constr. Steel Res. 64 (2008) 766–778.
[7] A.D. Martins, D. Camotim, P.B. Dinis, Local-distortional interaction in cold-formed steel beams: behaviour, strength and DSM design, Thin-Walled Struct. 119 (2017) 879–901.
[8] P. Kyvelou, L. Gardner, D. Nethercot, A. Finite element modelling of composite cold-formed steel flooring systems, Eng. Struct. 158 (2018) 28–42.
[9] G.Y. Matsubara, E. Batista, M. De, G.C. Salles, Lipped channel cold-formed steel columns under local-distortional buckling mode interaction, Thin-Walled Struct. 137 (2019) 251–270.
[10] W.S. Santos, A. Landesmann, D. Camotim, Distortional strength of end-bolted CFS lipped channel columns: experimental investigation, numerical simulations and DSM design, Thin-Walled Struct. 148 (2019) 1–25.
[11] O. Oey, J. Papangelis, Behaviour of cold-formed steel channels bent about minor axis, Thin-Walled Struct. 164 (2021) 107781.
[12] M. Gkantou, M. Bock, M. Theofanous, Design of stainless steel cross-sections with oustand elements under stress gradients, J. Constr. Steel Res. 179 (2021) 106491.
[13] Y. He, L. Dai, C. Ren, Buckling analysis of cold-formed steel lipped channel members under minor-axis eccentric load, J. Constr. Steel Res. 211 (2023) 108191.
[14] EN 1993-1-3 standard EUROPEAN COMMITTE FOR STANDARDIZATION. EN 1993-1-6, Eurocode 3: Design of Steel Structures - part 1.6: strength and stability of shell structures. Brussels, Belgium: CEN, 2007.
[15] J. Kim, J. Kim, Y.H. Lee, J. Baek, D. Kim, 'Flexural performance of a steel-concrete composite deck system strengthened with lattice reinforcement and hat-shaped shear connectors', J. Build. Eng. 97 (2024) 110913.
[16] ArcelorMittal. Trelifácil®, available at: https://brasil.arcelormittal.com/files/produtos-catalogos/4be03311-dbdf-4e83-85c8-b6d3b78f8d5c, access in 15th May 2024, 2024, In Portuguese.
[17] L.F. Favarato, Dimensionamento de lajes com vigotas treliçadas com forma em perfil u formado a frio. Trabalho de Conclusão de Curso (Graduação) – Departamento de Engenharia Civil, Universidade Federal do Espírito Santo, Vitória, ES, Brazil, 2018. In Portuguese.
[18] L.F. Favarato, A.F.G. Calenzani, J.C. Vianna, E. Junges, J.A. Ferrareto, Evaluation of the resistance of trussed slabs with steel formwork in cold formed U profile, Lat. Am. J. Solids Struct. 16 (2019) e178.
[19] A.V.S. Gomes, D.C.M. Candido, L.F. Favarato, J.A. Ferrareto, J.C. Vianna, A. F. Calenzani, Numerical and experimental study of a cold formed steel profile employed in steel-concrete composite ribbed slabs, in: Proceeding of the 8$^{\text{the}}$dition of *CONSTRUMETAL 2019 - Congresso Latino-Americano da Construção Metálica*, 2019. São Paulo, SP, Brazil.

[20] L.F. Favarato, A.V.S. Gomes, D.C.M. Candido, J.A. Ferrareto, J.C. Vianna, A.F. G. Calenzani, Proposition of a simplified analytical design procedure for lattice girder slabs with shuttering in cold-formed steel lipped channel section, Rev. IBRACON Estrut. Mater. 13 (5) (2020) 2020, vn.

[21] A.V.S. Gomes, D.C.M. Candido, L.F. Favarato, J.A. Ferrareto, J.C. Vianna, A.F. G. Calenzani, Finite element modeling of a cold-formed steel profile employed in composite ribbed slabs, Rev. Estrut. Aço – REA 11 (1) (2022) 60–80.

[22] L.F. Favarato, A.V.S. Gomes, D.C.M Candido, J.A. Ferrareto, J.C. Vianna, A.F. G. Calenzani, On the composite behavior of a rebar truss ribbed slab with incorporated shuttering made of lipped channel section, J. Build. Eng. 55 (2022) 104663.

[23] D.C.M. Candido, A.V.S. Gomes, L.F. Favarato, J.A. Ferrareto, J.C. Vianna, A.F. G. Calenzani, Flexural behavior of composite ribbed slabs employing cold-formed steel lipped channels, Eng. Struct. 298 (2024) 117070.

[24] ANSYS® 2020R1. *ANSYS® Academic Research Mechanical*, Release 2020R1.

[25] M.R. Haidarali, D.A. Nethercot, Finite element modelling of cold-formed steel beams under local buckling or combined local/distortional buckling, Thin-Walled Struct. 49 (12) (2011) 1554–1562.

[26] J. Ye, I. Hajirasouliha, J. Becque, K. Pilakoutas, Development of more efficient cold-formed steel channel sections in bending, Thin-Walled Struct. 101 (2016) 1–13.

[27] *Design of cold-formed steel structures*. ABNT NBR 14762, Rio de Janeiro, RJ, Brazil, Associação Brasileira de Normas Técnicas, 2010, In Portuguese.

[28] Z. Li, B.W. Schafer, Buckling analysis of cold-formed steel members with general boundary conditions using CUFSM conventional and constrained finite strip methods, in: International Specialty Conference on Cold-Formed Steel Structures, 2010.

[29] B.W. Schafer, S. Ádány, Buckling analysis of cold-formed steel members using CUFSM: conventional and constrained finite strip methods, in: Proceeding of the 18th International Specialty Conference on Cold-Formed Steel Structures, 2006. Orlando, Florida.

[30] *Eurocode 3: Design of Steel Structures - part 1.6: strength and stability of shell structures.* EN 1993-1-6, Brussels, Belgium, European Committe for Standardization, 2007.